Preliminary Thermal Analysis of Small Satellites

Casper Versteeg* and David L. Cotten, PhD†
Small Satellite Research Laboratory, The University of Georgia, Athens, Georgia, 30602

Small satellites lend themselves well to numerical modeling due to their size. Approximations that would be inappropriate for larger spacecraft can provide valuable insight at this scale, especially for thermally conductive materials. More accurate approximations can be obtained by progressively increasing the level of complexity of these models through the addition of more nodes. More sophisticated models also serve to validate previous numerical models. Inclusion of the beta angle as an independent variable, besides time, gives better insight in the lifetime temperature profile of the satellite, which have all been implemented in MATLAB.

Nomenclature

β	=	Beta angle, superscript star (*) denotes critical beta angle ($^\circ$)
R	=	Radius of Earth, ~ 6873km
h	=	Altitude (m)
f_E	=	Eclipse fraction (unitless)
a	=	Albedo factor (unitless)
$\dot{q}$	=	Heat flux ($\mathrm{W} \cdot \mathrm{m}^{-2}$)
$\dot{Q}$	=	Rate of heat transfer (W)
$\hat{s}$	=	Solar heating rate step multiplier (unitless)
τ	=	Orbital period (s)
$\alpha,\ \varepsilon$	=	Absorptivity, emissivity (unitless)
T	=	Temperature (K, unless otherwise noted)
t	=	Time (s)
σ	=	Stefan-Boltzmann constant, $\sim 5.67 \cdot 10^{-8} \mathrm{W} \cdot \mathrm{m}^{-2} \cdot \mathrm{K}^{-4}$
A	=	Area (m^2)
F	=	View factor (unitless)
$\odot$	=	Subscript, astronomical sign for Sun
$zen,\ nad$	=	Subscripts for Zenith and Nadir sides
$-/+v$	=	Subscripts for negative and positive velocity pointing sides
N/S	=	Subscripts for North and South pointing sides

I. Introduction

THE University of Georgia is currently developing two CubeSat class satellites for which these models have laid the groundwork for more complicated simulations. Because of the small scale of the 3U CubeSats in question (the Spectral Ocean Color sat, or SPOC, and Multi-view Onboard Computational Imager, or MOCI) small-scale numerical models with lumped mass assumptions can give valuable insight into the thermal behavior of these systems and the temperature ranges that can be expected on-orbit. Because of the similarities between these missions, these models serve as a baseline for both satellites.

Large satellite thermal analysis often involves complicated computer models or finite element analysis (FEA) in order to give an accurate temperature profile of a system [4]. As lumped mass approximations break down and temperature gradients inside structures and electronics become harder to model, these types

*Mechanical Team Lead, Small Satellite Research Laboratory, 175 International Dr. Athens, GA 30605, undergraduate.
†Research Scientist, Geography Department, 210 Field Street, Athens, Georgia, 30602

of simulations become too time-consuming to model in MATLAB. With the small size of CubeSat class satellites, this is avoided as radiating lumped mass criteria are frequently met by default [1].

II. Single-Node Analysis

To develop a baseline understanding of modeling the thermally dynamic environment of low earth orbit (LEO), a single-node lumped mass analysis was performed. This models the satellite as a sphere in a circular 400 km orbit around Earth. In building the heat transfer model, orbital inclination is modeled in the beta angle.

A. Beta Angle

Geometrically, the beta angle is defined as the angle between the sun-vector and the orbit plane (Figure 1a). Because there is no external influence to keep the orbital plane aligned with the sun-vector, the beta angle will vary over the course of a year. While the beta angle has a theoretical range of $\pm 90°$, for modeling the ISS orbit this range is realistically closer to $\pm 75°$ [6]. The beta angle has a strong implication on orbital heating rates, particularly when it comes to time spent in Earth's eclipse.

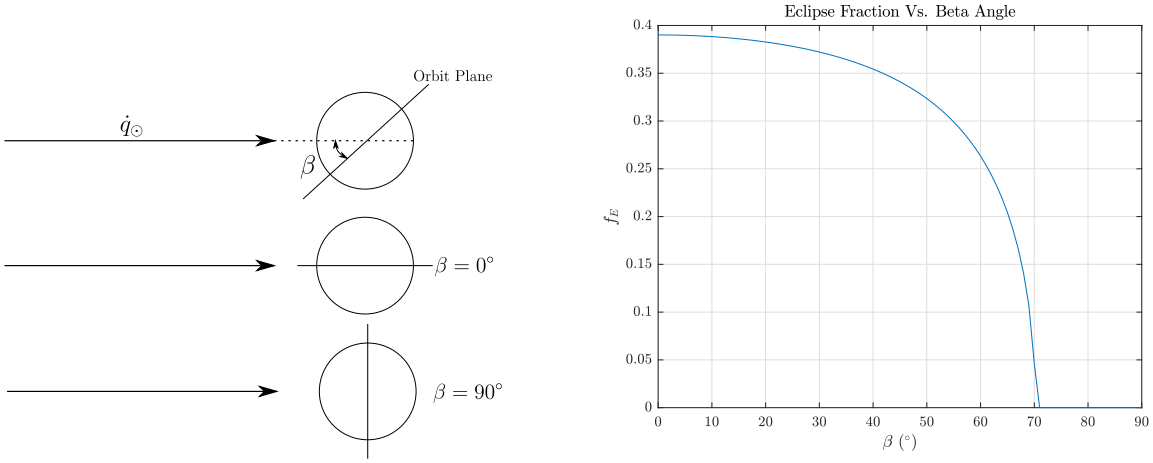

(a) Geometry **(b) Eclipse fraction Vs. beta angle**

Fig. 1 Geometric definition of beta angle

For a beta angle of $\pm 90°$, the sun-vector "sees" the entire orbit plane as a flat disk. This has the direct consequence that the satellite in orbit will be constantly exposed to sunlight, spending no time in eclipse. As the beta angle decreases the orbit plane will eventually intersect the horizon of the Earth at which point eclipse will be a factor to consider. This angle is defined as the critical beta angle [4]

$$\beta^* = \sin^{-1}\left(\frac{R}{R+h}\right) \tag{1}$$

This critical beta angle will give a piece-wise function describing the fraction of time in an orbit spent in eclipse

$$f_E = \begin{cases} \frac{1}{180°}\cos^{-1}\left(\frac{\sqrt{h^2+2Rh}}{(R+h)\cos(\beta)}\right) & |\beta| < \beta^* \\ 0 & |\beta| \geq \beta^* \end{cases} \tag{2}$$

The eclipse fraction itself governs the governing heat transfer equation on the satellite structure, as it dictates the time for which some heat transfer parameters are active. A plot of Eq. 2 is shown in Figure 1b

B. Heating Rates

Beyond orbital geometry, the beta angle also has an implication on heating rates in orbit. Besides solar radiation, a spacecraft in orbit will also experience heating from Earth infrared (IR), sunlight reflected from

the surface (Albedo) and heat generated internally. Both IR and Albedo heating rates are influenced by the beta angle. The following values are used in modeling albedo and IR, providing 3.3-σ accuracy values over a 90 minute period [4].

$$a = \begin{cases} 0.14 & \beta < 30^\circ \\ 0.19 & \beta \geq 30^\circ \end{cases} \tag{3}$$

$$\dot{q}_{IR} = \begin{cases} 228\text{W} \cdot \text{m}^{-2} & \beta < 30^\circ \\ 218\text{W} \cdot \text{m}^{-2} & \beta \geq 30^\circ \end{cases} \tag{4}$$

Important to note is that the IR flux has already been corrected for Earth's emissivity. The final piece to a full heat transfer model is the satellites own radiation. Per the Stefan-Boltzmann law, the spacecraft is assumed to radiate heat to deep space.

For an accurate on-orbit representation of temperature, the model must adapt the heating rates when the satellite enters eclipse. All solar heating rates must be removed during this time, which includes solar radiation and Albedo. If the model is initialized at solar noon (Figure 2), then solar radiation can be parameterized in terms of the orbit period and the eclipse fraction, for a given beta angle

$$\hat{s}(t) = \begin{cases} 1 & \frac{\tau}{2}(1 - f_E) > t > \frac{\tau}{2}(1 + f_E) \\ 0 & \text{else} \end{cases} \tag{5}$$

Adding this function to the heat transfer model will "turn off" the solar radiation when the satellite is set to enter eclipse, and "turn on" solar radiation when it leaves eclipse.

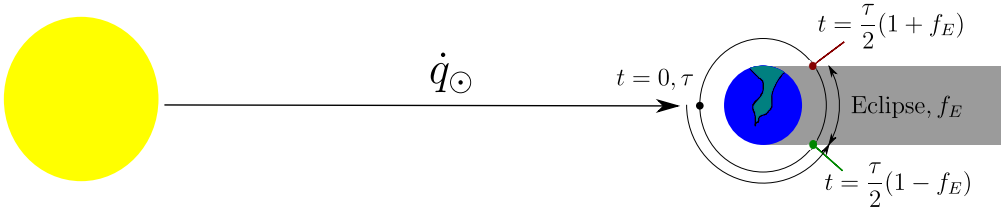

Fig. 2 Initialized model

For the single-node model, the satellite is modeled as a sphere where the assumption is made that the sphere has the same surface area as a 3U CubeSat. This means the incident radiation profiles are disks, but the total radiating surface is the complete spherical surface. For a 3U CubeSat, this works out to a sphere with a diameter of approximately 21.11 cm.

C. Heat Transfer Model

A complete single-node heat transfer energy balance can be set up using the parameters defined above. Figure 3 shows a complete diagram with all heat loads, which will serve as a guide for building the governing equation.

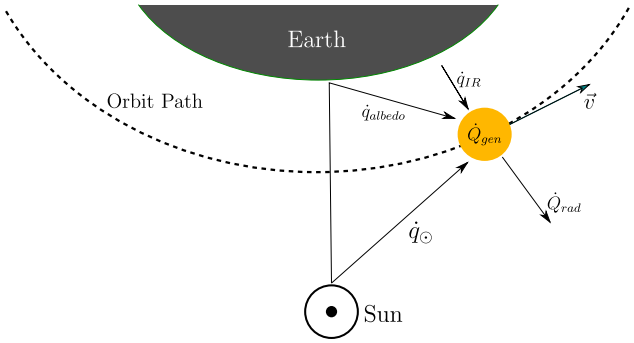

Fig. 3 Diagram representation of heat transfer model

The incident heat can be taken as the sum of solar radiation, IR and Albedo. Since the Albedo constant is a fraction of the total solar radiation reflected off Earth's surface, Albedo can be bundled with solar radiation. Note, this is only valid for a lumped mass model where internal temperature gradients are ignored. The incident heat equation, as one side of the complete energy balance, is

$$\dot{Q}_{in} = \dot{Q}_{IR} + \dot{Q}_{\odot} + \dot{Q}_{albedo} + \dot{Q}_{gen} = \dot{q}_{IR} A_{IR} + (1+a)\dot{q}_{\odot}\hat{s}A_{\odot}\alpha + \dot{Q}_{gen} \tag{6}$$

The area terms in this equation are dependent on the actual area exposed to the particular type of radiation. For the single-node model, all areas in the above equation are the area of the disk profile. [3] Since the radiation leaving the satellite is described simply by the Stefan-Boltzmann law, the total heat rate on the satellite is given by the energy balance

$$\dot{Q} = \dot{Q}_{in} - \dot{Q}_{rad} = \dot{q}_{IR} A_{IR} + (1+a)\dot{q}_{\odot} A_{\odot}\hat{s}\alpha + \dot{Q}_{gen} - A_s \sigma \varepsilon T^4 \tag{7}$$

This equation involves aborptivity and emissivity values that depend on the thermo-optical properties of the spacecraft. To remain conservative in the temperature estimates, these are taken as 0.96 and 0.90, respectively. This is to model the satellite as if coated in Aeroglaze Z306 black paint, for its high absorptivity. [2] Realistically, more favorable surface properties can be obtained through anodization, but this provides a good initial estimate.

To solve this model for temperature, it can be discretely integrated using the specific heat formula

$$\dot{Q} = c_p m \frac{dT}{dt} \approx c_p m \frac{\Delta T}{\Delta t} \tag{8}$$

which requires an assumption of material for the specific heat. Since the structure of the satellite is primarily Aluminium 6061-T6, this is the value assumed for the specific heat. The mass in this equation is taken to be the maximum mass of a 3U CubeSat (4 kg).

For smaller time-steps the approximation in Eq. 8 becomes more accurate, as the change in temperature over time approaches the exact derivative as the time-step approaches zero. This equation can be solved for temperature, noting that the total heat rate is a function of time.

$$T_{i+1} = T_i + \frac{\Delta t}{c_p m}\dot{Q}_i \tag{9}$$

Here, the index i indicates the temperature and heat rate at a discrete time t_i. The model is initialized such that $T(t_0) = 293.15\text{K}$, with heating rates determined at every time-step to determine the temperature T_{i+1}.

D. Results

The model as described above was created in MATLAB. It includes an internally generated heat load ($\dot{Q}_{gen}$) of 15.71W, based on the power budget. To remain conservative, this assumes 0% efficiency, and maximum power draw over all modes of the satellite. Furthermore, to account for variability in solar heat load through the seasons, the model is run separately in a "hot" case (corresponding to winter in the Northern hemisphere, $\dot{q}_{\odot,hot} = 1414\ \text{W}\cdot\text{m}^{-2}$) and "cold" case (summer in Northern hemisphere, $\dot{q}_{\odot,cold} = 1322\ \text{W}\cdot\text{m}^{-2}$).

Running the simulation in both hot and cold cases will provide an initial estimate for the temperature ranges that can be expected for the satellite. Because this model is spherical it does not incorporate changing area terms, or changes in projected area, which will have a tendency to narrow the expected temperature range. However, the single-node model should give an adequate initial estimate for this range.

The results from this analysis are shown in Figure 4. In line with expectations from Eq. 7, the cold-case temperature is always lower than the hot-case. The model tends to stabilize rather quickly, because of the small mass of the satellite. After running the simulation for five orbits, the difference between consecutive peaks is only about 0.03%, which is adequate for calling the model to be in a steady-dynamic state.

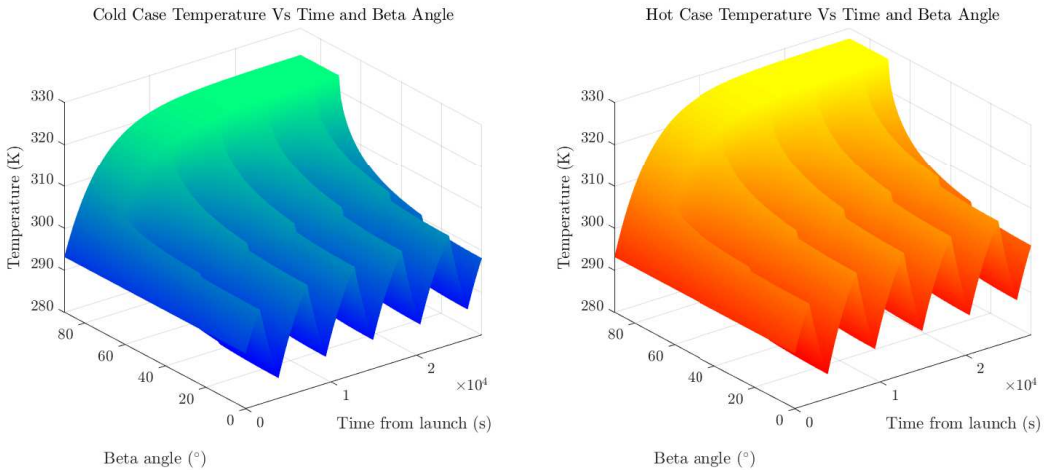

Fig. 4 Single-node results, left: cold, right: hot

As can be expected, the overall temperature of the spacecraft becomes higher as the beta angle increases. The satellite spends less time in eclipse at higher beta angles, so heating rates become low enough that the satellite can cool. Once the beta angle exceeds the critical beta angle (about 70.9°) the spacecraft is in continuous sunlight, and will thus reach steady-state under those heating rates, shown as a constant temperature plateau.

The dynamic behavior of the model exhibits a clear fourth-order polynomial behavior, as is expected from the Stefan-Boltzmann law. Effects of initial conditions (assumed here at 291.15 K) disappear quickly, most likely due to the small mass of the satellite. The $\beta = 30°$ marks a clear discontinuity due to the sudden switch in heating rates from Eq. 3, 4. Overall, this model behaves as expected.

III. Six-Node Analysis

In an effort to remove some of the assumptions in the single-node analysis, and increase the accuracy of the temperatures, a six-node model was developed. Instead of a single, spherical node model, this models each face of the satellite as its own node to compose a "box". This introduces some complexity over the single-node analysis, namely the consideration of view factors, and conduction between nodes. These nodes are still considered lumped masses, so internal temperature gradients are ignored.

A. Model Definition

While the governing equation will be mostly similar to that for the single-node model in Eq. 7, each of the sides of the six-node model will have some slight alterations to the specifics this equation. Each of these sides will henceforth be referred to by its designation per Figure 5, with each side denoted by a subscript as defined in the nomenclature.

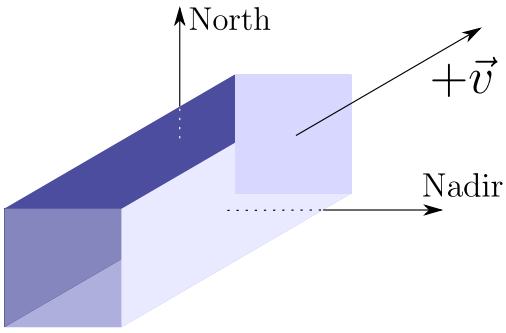

Fig. 5 Six-node side naming convention

Each of the sides is modeled as a lumped mass with a surface area equal to what it would actually be on a 3U CubeSat. Leaving this definition open allows for easy switching between orbit orientation. The 4 kg total mass of the satellite is distributed among the nodes such that the mass-area ratio remains constant. The same 15.71W of internally generated heat from the single-node model is distributed in a similar way. It should be noted here that all internal radiation (e.g. between the Nadir face and the Zenith face) is ignored.

For this model, all 3U faces of the satellite will be covered in photo-voltaic panels. This will impact the thermo-optical properties of those sides. While all other surfaces are assumed to have the same thermo-optical properties as the single-node model, these will have to be corrected for the photo-voltaic panels. Assuming seven panels per side, each with an absorptivity and emissivity of 0.92 and 0.85, respectively, an area weighted average is used to determine the overall thermo-optical properties of these sides. [5]

B. View Factors

Because the six-node model lacks the symmetry assumed in the single-node model, view factors are used to determine which sides are receiving solar radiation at what time. The view factor from one surface to another is defined as [3]

$$F_{1\to 2} = \frac{\cos(\theta_1)\cos(\theta_2)}{\pi r^2} dA_2 \tag{10}$$

Wherein the assumption can be made that $dA_2 \approx A_s$, because A_1 is the surface area of the Sun, which is much greater. Furthermore, because $\theta_1 << 1$, $\cos(\theta_1) \approx 1$. To retain the solar heating rates as defined in the single-node analysis, any distance dependency is removed.

The incident angle is a function of time, as the satellite progresses through the orbit, and must be piece-wise as some sides can be out of sunlight under certain conditions. A correction can be made to the view factors to account for the beta angle. As the beta angle increases, more of either the North or South faces becomes visible as the spacecraft progresses through an orbit. A geometric derivation of view factors leads to the following set of piece-wise equations

$$F_{zen} = \begin{cases} \cos\left(\frac{2\pi}{\tau}t\right)\cos(\beta) & \frac{\tau}{4} > t > \frac{3\tau}{4} \\ 0 & \text{else} \end{cases} \tag{11}$$

$$F_{-v} = \begin{cases} \sin\left(\frac{2\pi}{\tau}t\right)\cos(\beta) & t < \frac{\tau}{2}(1-f_E) \\ 0 & \text{else} \end{cases} \tag{12}$$

$$F_{+v} = \begin{cases} -\sin\left(\frac{2\pi}{\tau}t\right)\cos(\beta) & t > \frac{\tau}{2}(1+f_E) \\ 0 & \text{else} \end{cases} \tag{13}$$

$$F_{nad} = \begin{cases} -\cos\left(\frac{2\pi}{\tau}t\right)\cos(\beta) & \begin{cases} \frac{\tau}{4} < t < \frac{\tau}{2}(1-f_E) \\ \frac{\tau}{2}(1+f_E) < t < \frac{3\tau}{4} \end{cases} \\ 0 & \text{else} \end{cases} \tag{14}$$

$$F_{N/S} = \begin{cases} \sin(\beta) & \frac{\tau}{2}(1-f_E) > t > \frac{\tau}{2}(1+f_E) \\ 0 & \text{else} \end{cases} \tag{15}$$

The view factor equations above are all as seen from the Sun, dropping the astronomical sign from the subscript to reduce notation. It can be shown, that all other view factors (i.e. those from Earth to any of the sides around Nadir) are approximately zero, and can be ignored.

C. Heat Transfer Model

As in the single-node analysis, a governing energy balance can be set up. In this case, it will involve a set of six equations, each modeling the energy balance for each of the six sides of the box. This must involve a conduction model between each of the six sides. This can be captured using a thermal contact conductance coefficient k, and the interface area between the relevant sides. Contact conductance is well documented in literature, where it is controlled for contact pressure and surface roughness. To create a conservative model, a low value of 400 $\mathrm{Wm^{-2}K^{-1}}$ based on [4] is chosen for this analysis. The set of heat transfer equations is as follows:

$$\dot{Q}_{zen} = F_{zen}A_{zen}\dot{q}_{\odot}\alpha + k\sum_{i=1}^{4} A_i(T_i - T_{zen}) - \sigma\varepsilon_{zen}A_{zen}T_{zen}^4 \tag{16}$$

$$\dot{Q}_{-v} = F_{-v}A_{-v}\dot{q}_{\odot}\alpha + k\sum_{i=1}^{4} A_i(T_i - T_{-v}) - \sigma\varepsilon_{-v}A_{-v}T_{-v}^4 \tag{17}$$

$$\dot{Q}_{+v} = F_{+v}A_{+v}\dot{q}_{\odot}\alpha + k\sum_{i=1}^{4} A_i(T_i - T_{+v}) - \sigma\varepsilon_{+v}A_{+v}T_{+v}^4 \tag{18}$$

$$\dot{Q}_{nad} = (F_{nad} + a)A_{zen}\dot{q}_{\odot}\alpha + \dot{q}_{IR}A_{nad} + k\sum_{i=1}^{4} A_i(T_i - T_{nad}) - \sigma\varepsilon_{nad}A_{nad}T_{nad}^4 \tag{19}$$

$$\dot{Q}_{N} = F_{N}A_{N}\dot{q}_{\odot}\alpha + k\sum_{i=1}^{4} A_i(T_i - T_{N}) - \sigma\varepsilon_{N}A_{N}T_{N}^4 \tag{20}$$

$$\dot{Q}_{S} = k\sum_{i=1}^{4} A_i(T_i - T_{zen}) - \sigma\varepsilon_{S}A_{S}T_{S}^4 \tag{21}$$

Each of the above equations is discretely integrated in a similar fashion as Eq. 9. The six-node model employs the conduction model in such a way, that each side conducts only to the sides that are touching it directly with an interface area A_i. For example, the Nadir side will conduct directly to $+v$, $-v$, North and South.

The equations above also lend themselves well to changing the orientation of the satellite as it is marched forward in time through its orbit. By simply re-designating the sides as shown in Figure 5, the model can be changed quite simply by changing the area and thermo-optical terms in the heat transfer equations above.

D. Results

This model will yield a set of results where the temperature profile again varies with time as well as beta angle. With the introduction of six nodes, there are now many more variables for which this model can be controlled, although the most interesting one is temperature ranges. As this is meant to be a continuation of the single-node model, the expectation is that the temperature ranges are more refined in this model than the previous. Figure 6 shows the results of both the time-beta-temperature plot (a), as well as the temperature ranges per beta angle (b).

The results in Figure 6a show behavior that is absent in the single-node analysis. As beta angle increases, the temperature peaks increase, reach a maximum, and decrease again. This is a perfect example of the area-dependent effects of this model, where the projected area of the satellite towards the sun increases with beta angle, thereby increasing the temperature observed. The temperature reaches another maximum with increasing beta angle as the eclipse fraction decreases to zero. While the analysis does not converge quite as quickly to steady-dynamic as the single-node analysis, the difference between peaks in this model is only about 0.4%.

Each of the points in Figure 6b resembles the hot and cold temperature extrema of a node in this model, which are overlaid with the temperature extrema from the single-node analysis, to confirm agreement. To

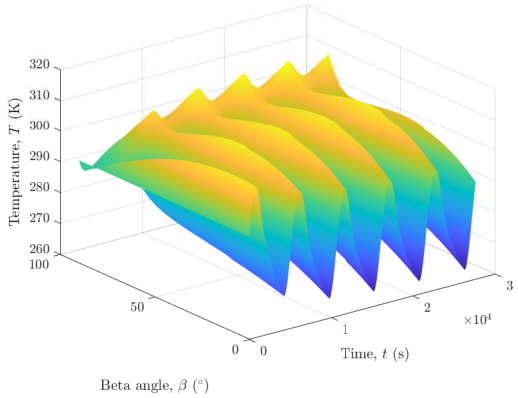

(a) Temperature result plot: Zenith, cold

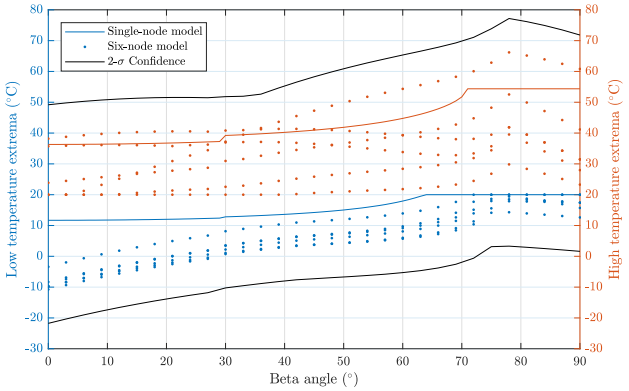

(b) Six-node temperature extrema overlaid with single-node temperature range

Fig. 6 Six-node results

make these results viable for acceptance testing procedures, simulation temperatures will be padded by 11°C to bring them within a 2-σ confidence interval [4, 7]. This puts the temperature range estimate of the satellite at -22°C to 77°C, which is an adequate estimate for this level of simulation complexity.

IV. Conclusion

A general trend that is observed from these models, is that the satellite's temperature responds very quickly to changes in the heat load, because of the small mass of the system. In general, the satellite will reach a steady temperature range after around five orbits, where all of the effects of the initial temperature will have disappeared from the transient solution. At orbit five, the difference between peak values of the temperature changes on average by a value of around 0.4%, which can be considered steady for the purposes of this analysis.

The temperature fluctuations of all the models considered above are relatively in agreement. While differences are expected as the complexity of the models increases, the differences observed are within an expected range. While the generated heat load will, in reality, change as the satellite transitions between modes, the full power draw (assuming 0% efficiency) is always "on" in this analysis, providing a conservative estimate for the temperature, as heat loads are expected to be lower.

Further development of these satellite heat transfer models can involve finite element analysis, to provide a better approximation of internal temperature gradients. While it is possible to do this in MATLAB, it is not well equipped to handle discontinuities in the models, such as the interfaces between sides. Instead, these models can be developed in more specialized tools, such as Thermal Desktop.

Acknowledgments

The author would like to thank Dr. Benjamin Wagner, PE for double checking the work done in this manuscript. This research was made possible through funding by the University Nanosatellite Program and the Air Force Research Lab.

References

[1] *Small Satellite Thermal Modeling and Design at USAFA FalconSat-2 Applications*, 2002.

[2] Lord Corporation. *Aeroglaze® Z306 Flat Black Absorptive Polyurethane, Low Outgassing.* Erie, PA.

[3] Y. A. Çengel and A. J. Ghajar. *Heat and Mass Transfer: Fundamentals and Applications.* McGraw Hill Education, New York, NY, 5th edition, 2015.

[4] David G. Gilmore, editor. *Spacecraft Thermal Control Handbook*. The Aerospace Press, El Segundo, CA, 2nd edition, 2002. ISBN 978-1-884989-11-7.

[5] Spectrolab Inc. *28.3% Ultra Triple Junction (UTJ) Solar Cells*. Sylmar, CA, 2010.

[6] Charles A. Jacobson Jr and Robert A. Rudd. Development of space station loads due to on-orbit thermal environments. 1996.

[7] E. Perl and James R. Horejsi. Test requirements for launch, upper-stage and space vehicles. Technical report, Space and Missile Systems Center Air Force Command, El Segundo, CA, 2006.